Increased neutralization of SARS-CoV-2 Delta variant by nanobody (Nb22) and the structural basis

Xilin Wu[1,2]†, Yaxing Wang[3]†, Lin Cheng[4]†, Linjing Zhu [2]†, Sen Ma[3], Bilian Huang[1], Shijie Xu[5], Haixia Shi[5], Doudou Zhang[5], Linshuo Liu[5], Waqas Nawaz[1], Sheng Ye[3,6*], Zhiwei Wu[7, 8, 9,10*]

1. Center for Public Health Research, Medical School, Nanjing University, Nanjing, P.R. China.

2. Department of Antibody, Abrev Biotechnology Co., Ltd. Nanjing, P.R. China.

3. Tianjin Key Laboratory of Function and Application of Biological Macromolecular Structures, School of Life Sciences, Tianjin University, 92 Weijin Road, Nankai District, Tianjin 300072, P.R. China.

4. Institute for Hepatology, National Clinical Research Center for Infectious Disease, Shenzhen Third People's Hospital, Shenzhen, P.R. China.

5. Department of Antibody, Y-clone Medical Science Co. Ltd. Suzhou, P.R. China.

6. Life Sciences Institute, Zhejiang University, Hangzhou, 310058 Zhejiang, P.R. China.

7. School of Life Sciences, Ningxia University, Yinchuan, P.R. China.

8. Jiangsu Key Laboratory of Molecular Medicine, Medical School, Nanjing University, Nanjing, P.R. China.

9. State Key Laboratory of Analytical Chemistry for Life Science, Nanjing University, Nanjing, P.R. China.

10. Lead contact

†These authors contributed equally to this work.

*Corresponding author: Z. Wu, E-mail: wzhw@nju.edu.cn and S. Ye, E-mail: sye@tju.edu.cn

Mailing address: School of Life Sciences, Ningxia University, Yinchuan, 750021, China.

Phone: +86 (25) 8368-6092. Fax: +86 (25) 8359-6023.

Abstract (202 words)

Delta variant, also known as B.1.617.2, has become a predominant circulating variant in many countries since it first emerged in India in December 2020. Delta variant is less sensitive to serum neutralization from COVID-19 convalescent individuals or vaccine recipients, relative to Alpha strains. It was also resistant to neutralization by some anti-receptor binding domain (RBD) and anti-N-terminal domain (NTD) antibodies in clinics. Previously, we reported the discovery of nanobodies isolated from an alpaca immunized with spike protein, exhibiting ultrahigh potency against SARS-CoV-2 and its mutated variants, where a novel inhalable bispecific Nb15 protected SARS-CoV-2 infection in hACE2 mice. Here, we found that Nb22-Fc, among our previously reported nanobodies, exhibited 8.4-fold increased neutralization potency against Delta variant with an IC_{50} value of 0.41 ng/ml (5.13 pM) relative to Alpha variant. Furthermore, our crystal structural analysis reveals that the binding of Nb22 on SARS-CoV-2 RBD effectively blocks the binding of RBD to ACE2 during virus infection. Furthermore, the L452R mutation in RBD of Delta variant forms an additional hydrogen bond with the hydroxy group of T30 of Nb22, leading to the increased neutralization potency of Nb22 against Delta variant. Thus, Nb22 is a potential therapeutic agent against SARS-CoV-2, especially the highly contagious Delta variant.

Keywords: SARS-CoV-2, Delta variant, B.1.617.2, Nanobody, Nb22, RBD, Structure

Introduction:

SARS-CoV-2 has given rise to the COVID-19 pandemic [1], resulting in massive disruption of social and economic activities. Global vaccination has since provided protection against the catastrophic outcome of the pandemic. However, a new wave of infection, mainly caused by Delta variant, is spreading rapidly worldwide [2-5]. The Delta variant, also known as B.1.617.2, was first identified in Indian in December 2020, characterized by the spike protein mutations T19R, L452R, T478K, D614G, P681R, D950N and a double deletion 157-158 [6]. Delta variant has become predominant in many countries, representing over 90% of daily new cases in Africa, Asia, Europe, North America between August 01 and September 01, 2021 (https://www.gisaid.org/hcov19-variants/). It has been designated as a Variant of Concern (VOC) and is believed to be 60% more transmissible than Alpha variant [7].

Delta variant also poses a challenge to the COVID-19 vaccines. The protective effectiveness of AstraZeneca and Pfizer vaccines against Delta variant was reduced to 60% and 88%, respectively [6, 7]. Neutralizing experiments indicated that AstraZeneca and Pfizer vaccine-elicited antibodies were less effective to Delta variant, with about 3-5 fold less potent than that against Alpha variant [7]. To date, over 2 billion doses of vaccines have been administrated worldwide and several antibodies drug, like Casirivimab and Imdevimab combination, Bamlanivimab and Etesevimab combination, and Sotrovimab, were approved for emergency use in the prophylaxis or treatment of SARS-CoV-2 infection [8, 9]. Whereas, vaccine breakthrough infection was recently reported worldwide [10], which was mainly caused by Delta variant. Death caused by Delta variant was increasing with 2.05% weekly change since August 16, 2021 (https://covid19.who.int/). Altogether, these findings highlight the urgent need to develop new anti-viral agents for the prophylaxis or treatment of the Delta variant infection.

Recent research indicated that the emerging Delta variant partially but significantly resists neutralization by mAbs, SARS-CoV-2 convalescent sera and vaccine-elicited

antibodies [11-13]. The K417N mutation in the spike protein could confer resistance to monoclonal antibodies Imdevimab and Casirivimab as well [7, 11, 14, 15]. Some mAbs, including Bamlanivimab, lost binding to the spike and failed to neutralize Delta variant [16]. B1-182.1 and A23-58.1, recently isolated from convalescent donors, exhibited ultrapotent neutralization against Delta variant with IC_{50} values of 1.0 and 1.6 ng/ml, respectively [16].

To date, a growing number of nanobodies, single-domain fragments of camelid heavy-chain antibodies or VHH, were described for the prophylaxis or treatment of SARS-CoV-2 infection. However, rarely nanobodies with potent neutralization against Delta variant were reported [17-24]. Previously, we identified three ultrapotent nanobodies including Nb15-Fc, Nb22-Fc and Nb31-Fc against the initial strain of SARS-CoV-2, variant Wuhan-Hu-01 (WH01), with IC_{50} values of ~1 ng/ml. These antibodies were isolated from an alpaca immunized with spike protein of WH01 variant. Nb15-Fc with the highest neutralization potency against WH01 variant was selected for further investigation. Of note, intranasal delivery of Nb15 could protect hACE2 mice infected by WH01 variant [25]. In the current report, we compared the neutralizing potency of the aforementioned nanobodies against various circulating SARS-CoV-2 variants. Like most anti-RBD antibodies, Nb15-Fc and Nb31-Fc exhibited reduced neutralization against Delta variant as compared to WH01 variant or Alpha variant. Surprisingly, Nb22-Fc exhibited increased neutralization potency against Delta variant comparing to against WH01 variant, to which the antibody was originally raised. It is uncommon that an anti-RBD antibody exhibited increased potency against Delta variant relative to Alpha variant. The binding characterization and crystal structural analysis were conducted to further explore the potential mechanism.

Overall, Nb22-Fc exhibits ultrapotent neutralization and warrants further development for the prophylaxis or treatment of SARS-CoV-2 circulating variants, especially the current predominant Delta variant. The structural analysis may further guide the rational design of pan-coronavirus vaccines and therapeutics.

2. Materials and Methods

2.1. Expression, of nanobodies

The Fc1 gene (CH2-CH3) of the human monoclonal antibody was fused with the VHH gene of nanobodies (named as Nb-Fc) to assist the purification and prolong the half-life of the Nb-Fc antibody, following our previously published protocol [26]. The Nb-Fcs were finally cloned into the pcDNA3.4 eukaryotic expression vector (Invitrogen), which were transfected into 293F cells (cat.# R79007, Thermo Scientific) to produce Nb-Fcs. Nb fused with Fc was purified using Protein G (cat.# 20399, Thermo Scientific).

2.2 Neutralization activity of nanobodies against pseudovirus

Pseudovirus neutralization assay was carried out following our previously published protocol [25], with the follow modifications. Briefly, pseudovirus of SARS-CoV-2 variants was produced by co-transfection of pNL4-3.Luc.R-E-, an HIV-1 NL4-3 luciferase reporter vector that comprises defective Nef, Env and Vpr (HIV AIDS Reagent Program), and pCDNA3.1 (Invitrogen) expression vectors encoding the spike proteins of respective variants into 293T cells (ATCC). Supernatants containing pseudovirus were collected after 48 hour (h), and viral titers were determined by luciferase assay in relative light units (Bright-Glo Luciferase Assay Vector System, Promega Biosciences). Human codon optimized S genes of SARS-CoV-2 variants were synthesized, and the corresponding pseudoviruses were produced following the above protocol. For neutralization assay, SNB02, an Nb-Fc specific against SFTSV [26], served as a negative control. Neutralization assays were conducted by incubating pseudovirus with serial dilutions of purified nanobodies at 37 °C for 1 h. HEK293T-ACE2 cells (cat.# 41107ES03, Yeasen Biotech Co., Ltd. China) (approximately 1.5×10^4 per well) were added in duplicate to the virus-antibody mixture. Half-maximal inhibitory concentrations (IC_{50}) of the evaluated nanobodies were determined by luciferase activity 48 h following exposure to virus-antibody mixture, and analyzed by GraphPad Prism 8.01 (GraphPad Software Inc.).

2.3 Immunofluorescence and flow cytometric analysis.

Immunofluorescence and flow cytometric analysis were conducted following our previously published protocol [27], with minor modifications. Briefly, S gene sequences for SARS-CoV-2 spike protein of various SARS-CoV-2 variants were obtained from the GISAID website (https://gisaid.org). S genes were synthesized and constructed as expression plasmids by GenScript. The plasmids were transfected into 293T cells (ATCC) cultured in 12-well plates. Next, 48 hours post transfection, the cells were washed by PBS and fixed with 4% paraformaldehyde for 20 minutes at room temperature. The purified Nb-Fc was used to stain the 293T cells, followed by Alexa Fluor 488 AffiniPure goat Anti-human IgG (H+L) (1:500 dilution) (109-545-003, Jackson ImmunoResearch). For immunofluorescence analysis, the cells on the plate were examined and the images were acquired using an OLYMPUS IX73. For flow cytometric analysis, the cells were resuspended in 500 µl PBSF buffer (PBS+2% FBS) and analyzed using ACEA NovoCyte TM (Agilent Biosciences), non-transfected 293T cells served as a negative control.

2.4 Affinity determination by Bio-Layer Interferometry (BLI)

We measured antibody affinity using a ForteBio OctetRED 96 BLI (Molecular Devices ForteBio LLC, Fremont, CA) with shaking at 1,000 rpm at 25 ºC [25]. To determine the affinity of nanobodies, RBD protein was coupled to AR2G biosensor (cat.# 18-5092, Fortebio) using BLI instrument following the instruction of the amino coupling kit. Association of Nb-Fcs in a serial dilution was carried out before dissociation for 180 sec. After each cycle, the biosensors were regenerated through 3 brief pulses of 5 sec each with 100 mM pH 2.7 glycine-HCL followed by running buffer. The data were baseline subtracted before fitting using a 1:1 binding model and the ForteBio data analysis software. K_D, *Ka* and *Kd* values were determined by applying a global fit to all data.

2. 5. Expression and purification of RBD protein

The SARS-CoV-2 RBD was expressed using the Bac-to-Bac baculovirus system,. The pAcgp67-RBD (residues 333–530) plasmid with a C-terminal 8×His tag was transfected into Sf9 cells using Cellfectin II Reagent (Invitrogen) to produce the recombinant baculoviruses. After 3 rounds of amplification, Hi5 cells were infected with baculoviruses at MOI of 4 at a density of 2×10^6 cells/ml. The supernatants of cell culture containing the secreted RBD were harvested at 60 h after infection. The RBD was purified by Ni-NTA resin (GE Healthcare). Nonspecific contaminants were removed by washing the resin with 20 mM Tris-HCl, 150 mM NaCl, pH 7.5, and the target proteins were eluted with elution buffer containing 20 mM Tris-HCl, 150 mM NaCl, 500 mM imidazole, pH 7.5. The eluted proteins were further purified by Superdex 75 (GE Healthcare, USA) and stored in 20 mM Tris-HCl, 150 mM NaCl, pH 7.5.

2.6 Expression and purification of Nb22 for crystal structural analysis

The VHH gene for Nb22 was amplified by PCR and cloned into a pET21a vector with *Bam*H I and *Xho* I restriction sites. The recombinant plasmids were transformed into *Escherichia coli*. BL21 (DE3). The cells were cultured in LB medium and grown to $OD_{600} = 0.8$ at 37°C. Isopropyl-D-1-thiogalactopyranoside (IPTG) was added to a final concentration of 1.0 mM to induce the protein expression, and the cultures were grown at 16 °C overnight. Cells were harvested by centrifugation at 4,500 rpm for 15 min, re-suspended and homogenized in the lysis buffer containing 20 mM Tris-HCl, 150 mM NaCl, pH 7.5 using ultrasonic. Cell debris were removed by centrifugation at 18,000 rpm for 30 min. The supernatants were added to Ni- NTA resin (GE Healthcare, USA). The nonspecific contaminants were eluted by washing the resin with the lysis buffer containing 10 mM imidazole. The target protein with 6 x His tag, named as Nb22, were subsequently eluted with the lysis buffer containing 500 mM imidazole. Nb22 were eluted and purified by Superdex 75 (GE Healthcare, USA).

2.7 Crystallization, structural determination and data acquisition

The complexes were prepared by mixing SARS-CoV-2 RBD and Nb22 at a 1:1.2 molar ratio and incubating at 4 °C overnight. The complexes were further purified by Superdex 75 (GE Healthcare, USA) to remove the excess nanobody. The crystals were screened by vapor-diffusion sitting-drop method at 16˚C. The crystals appeared and reached their final size within 3 days in a well solution comprising 0.1 M HEPES (pH 7.0), 5% *v*/*v* (+/-)-2-Methyl-2,4-pentanediol (MPD) and 10% polyethylene glycol (PEG) 10000.

To collect data, a single crystal was mounted on a nylon loop and was flash-cooled with a nitrogen gas stream at 100 K. Diffraction data was collected on BL18U1 at Shanghai Synchrotron Radiation Facility (SSRF) at a wavelength of 0.97915 Å with a Pilatus3 6M image plate. Data were processed and scaled using the HKL3000 package [28]. The structure was elucidated using the molecular replacement (MR) method in PHASER program [29] with the structure of SARS-CoV-2 RBD (PDB code: 7CJF) [30] as the initial searching model. The model was built into the modified experimental electron density using COOT [31] and further refined in PHENIX [32]. The final refinement statistics were summarized in Table S1. Structural figures were prepared by PyMOL. Epitope and paratope residues, as well as their interactions, were identified by PISA (http://www.ebi.ac.uk/pdbe/prot_int/pistart.html) at the European Bioinformatics Institute.

2.8. Quantification and statistical analysis

All statistical analyses were carried out using GraphPad Prism 8.01 software (GraphPad) or OriginPro 8.5 software (OriginLab). ANOVA or Mann-Whitney test was performed for group comparisons. $P < 0.05$ was considered as statistically significant with mean ±SEM or mean ±SD.

3. Results

3.1 Potent neutralization of Delta variant by nanobodies

We previously reported the discovery and characterization of three potent neutralizing nanobodies against WH01 variant and the mutated variants with IC_{50} values of ~1ng/ml.

These three nanobodies, Nb15-Fc, Nb22-Fc and Nb31-Fc, were identified binding to RBD [25]. Neutralization experiments were further conducted to measure their activity against the circulating variants including variants of concern (VOC) comprising Alpha (B.1.1.7 with N501Y), Beta (B.1.351 with E484K and N501Y), Delta (B.1.617.2 with L452R and T478K) and Gamma (P.1 K417T, E484K and N501Y), as well as variants of interest (VOI) comprising Eta (B.1.525 with E484K), Iota (B.1.526 with E484K), Epsilon (B.1.429 with L452R), and Kappa (B.1.617.1 with L452R and E484Q) [2-5]. Nb15-Fc exhibited increased potency against Alpha variant, but decreased potency against Delta variant or Epsilon as compared with WH01 variant, the variant RBD used to select the nanobodies. Nb31-Fc exhibited reduced potency against Alpha, Delta and Epsilon variants relative to WH01 or D614G variant. Nb15-Fc and Nb31-Fc failed to neutralize other variants containing E484K/Q mutation (Fig. 1A-F). Surprisingly, Nb22-Fc exhibited around 2.5-fold increased neutralizing potency against Delta variant with an IC_{50} value of 0.41 ng/ml (5.13 pM) compared with variant WH01 with an IC_{50} of 1.01 ng/ml (12.63 pM). Notably, Nb22-Fc also exhibited around 8.4-fold increased neutralization potency against Delta variant relative to variant Alpha with an IC_{50} of 3.45 ng/ml (43.13 pM) (Fig. 1A-F). All three nanobodies failed to neutralize variants containing E484K/Q mutation, suggesting that E484K/Q mutation in RBD could lead to the resistance to all three nanobodies.

Altogether, Nb15-Fc presented the most potent neutralization against variant Alpha with an IC_{50} of 0.18 ng/ml, and Nb15-Fc and Nb31-Fc still retain potent neutralization of variants containing L452R and T478K mutations in RBD (Fig. 1E-F), though with reduced potency like most other anti-RBD antibodies [2, 7]. Of note, Nb22-Fc exhibited the most potent neutralization of variants Delta and Epsilon among three nanobodies (Fig. 1E-F).

3.2 Characterization of Nb22-Fc binding to RBD

To explore the characteristics of antibody binding to the RBD with respect to their neutralization of Delta variant, the interactions of three nanobodies with variant RBDs

were analyzed using biolayer interferometry (BLI). Nb15-Fc, Nb22-Fc and Nb31-Fc showed high affinity interactions with RBD of Delta variant at 1.86 nM, 0.31 nM and 0.31 nM, respectively (Fig. 2A-D). However, the ultrahigh affinity of Nb22-Fc and Nb31-Fc to RBD of Delta variant did not reflect the neutralization potency accordingly as Nb22-Fc neutralized Delta variant with markedly more potency than that of Nb31-Fc, suggesting that affinity is not the only factor dictating the neutralization activity. Furthermore, Nb22-Fc exhibited increased affinity with Delta variant RBD relative to other variant RBDs (Fig. 2A-D), which is in line with the increased potency conferred by Nb22-Fc against Delta variant as compared with variant Alpha.

Moreover, immunofluorescence analysis revealed that Nb22-Fc interacted specifically with spike protein from WH01, D614G, Alpha, Epsilon and Delta variants on the surface of transfected 293T cells, whereas no binding with the spike protein from other variants containing E484K/Q mutation (Fig. 2E). These results were substantiated by FACS results (Fig. 2F). Overall, these specific binding characteristics are consistent with its specific neutralization properties.

3.3 Structural analysis of RBD-Nb22 complex

Structural analysis of Nb22 interaction with RBD was performed to address the increased neutralization potency of Delta variant. We determined the crystal structure of RBD-Nb22 complex at a resolution of 2.7 Å (Fig. 3A and Table S1). Nb22 adopts a typical β-barreled structure, and contains three variable complementarity-determining regions (CDR) binding to RBD. The buried surface area (BSA) was 800 $Å^2$, and mainly constituted of hydrogen bonds and hydrophobic interactions. 14 residues constituting epitope of three CDRs were identified using a distance of <4 Å as the cutoff (Fig. 3B). For CDR1, T30 and S33 formed two hydrogen bonds with S494 of RBD, while the hydrophobic interactions included A32 and F34 of Nb22 and Y449, N450, L453, F490 and Q493 of RBD (Fig. 3C). N57 of CDR2 interacted with G485, C488 by hydrogen bonds, and the hydrophobic interactions were mediated by I56, E484 and Y489 (Fig. 3D). CDR3 was a relatively longer region with only one hydrogen bond (Y119 and

G446). The side chain of P104 inserted into the hydrophobic cavity formed by F101, R107, Y453 and F456 (Fig. 3E). Apart from the five hydrogen bonds in CDR regions, the interface of Nb22 and RBD was stabilized by three additional hydrogen bonds consisted of G1, S75, N450 and E484 (Fig. 3F). Interactions were also facilitated by the hydrophobic network constituted by P2, Q3, V4, G28, G29, R73 and D74 of Nb22 (Fig. 3G).

3.4 Nb22 blocks RBD binding to ACE2 and inhibits the Delta variant

Superimposition of the structure of Nb22-RBD complex and that of RBD-ACE2 (PDB code: 6MOJ) immediately elucidates the structural basis of neutralization, in which the binding of Nb22 to RBD effectively blocks the binding of RBD to ACE2 during virus infection. First, the binding site of Nb22 on RBD is partly overlapped with that of ACE2 (Fig. 4A). Second, the loop (V102-Y117) of Nb22 clashes with two α-helices of the N-terminus of ACE2 (Fig. 4B).

The structure of Nb22-RBD complex also elucidates why Nb22 can block the infection of Delta variant with increased binding affinity. Delta variant contains two distinct mutations, T478K and L452R. To assess whether these two sites affected the interaction between Nb22 and RBD, we generated the hydrogen and hydrophobic network using PISA (Supplementary Table S2). The T478 is located outside the CDR binding regions (Fig. 5A), and does not disturb the hydrogen bonding and hydrophobic interactions. Therefore, T478K mutation has no effect on Nb22 neutralization (Fig. 5B and 5C). L452 is located at the edge of the epitope region of CDR1 and participates in the hydrophobic interactions of the interface. Mutation of L452 to arginine (R), though a hydrophobic to basic change, does not perturb the hydrophobic interaction. Instead, the guanidine moiety of R452 forms an additional hydrogen bond with the hydroxyl group of T30 of Nb22, thus enhancing the binding affinity (Fig. 5A and C).

Discussion:

A small number of nanobodies with ultrahigh potency against SARS-CoV-2 and its variants have been described [16, 33, 34], whereas majority of the nanobodies rarely

neutralize the currently circulating Delta variant. Our results revealed that three previously reported nanobodies [25], retained ultrahigh potency in neutralization against SARS-CoV-2 Delta variant. Among them, Nb22-Fc with an IC_{50} value of 0.41ng/ml (5.13 pM) is outstanding with increased neutralization of Delta variant compared with that of Alpha variant. The binding of Nb22 to RBD provides mechanistic insight into the enhanced neutralization against Delta variant, suggesting that the increased binding affinity enhanced the neutralizing potency against Delta variant relative to Alpha variant (Fig. 1). Given that most anti-RBD, anti-NTD antibodies or convalescent sera or vaccine-elicited antibodies showed reduced neutralization of Delta variant relative to that of Alpha variant [2, 7], the increased neutralization activity of Nb22-Fc against Delta variant is particularly striking and prompted us to explore the structural basis of the phenomenon.

The structural analysis further explored the Nb22-RBD binding characteristics and the mechanisms of viral inhibition. Nb22 binding to RBD effectively blocked the binding of RBD to ACE2 during virus infection. The binding site of Nb22 on RBD is partly overlapped with that of ACE2 (Fig. 4A), and the loop (V102-Y117) of Nb22 clashes with two α-helices of the N-terminus of ACE2 (Fig. 4B). In addition, crystal structural analysis shows that T478K mutations of Delta variant are located outside 800 $Å^2$ buried surface area of Nb22 interacting with RBD and do not perturb the interaction between Nb22 and the RBD of Delta variant. Of note, the guanidine moiety in the L452R mutation forms an additional hydrogen bond with the hydroxyl group of T30 of Nb22, thus enhancing the binding affinity, suggesting the explanation of increased binding and neutralizing potency of Nb22 against Delta variant characterized with L452R and T478K mutations in RBD. Moreover, the BSA of Nb22-RBD (800 $Å^2$) is relatively large compared to reported neutralizing nanobodies (Table S3). When RBD mutates to L452R and T478K, the BSA extends from 800 $Å^2$ to 830 $Å^2$, which contributes to the higher binding.

Previously, we reported a bi-specific trimer configuration Nb_{15}-Nb_H-Nb_{15} based on

Nb15 nanobodies, which contains Nb15 specific for RBD and NbH specific for human serum albumin protein in blood [25]. Nb_{15}-Nb_H-Nb_{15} exhibited increased neutralization *in vitro* and half-life *in vivo*. Importantly, intranasal delivery of Nb_{15}-Nb_H-Nb_{15} resulted in the prevention and therapy of SARS-CoV-2 infection in hACE2 mice [25]. As such, we presume that Nb22 could also be engineered as Nb_{22}-Nb_H-Nb_{22} like Nb15 with both improved *in vivo* stability and neutralization. Accordingly, given ultrapotent neutralization of Nb22 against Delta variant with an IC_{50} value of 0.41 ng/ml, intranasal delivery of Nb_{22}-Nb_H-Nb_{22} could achieve similar therapeutic efficacy as Nb_{15}-Nb_H-Nb_{15} against Delta variant infection *in vivo*.

In summary, SARS-CoV-2 Delta variant is characterized by the substitutions of T478K and L452R in RBD, which are known to affect transmissibility of the virus as well as neutralization by antibodies [35]. Whereas unlike Nb15-Fc and Nb31-Fc, Nb22-Fc exhibited increased neutralization potency against Delta variant relative to other variants. Structural analysis provides a mechanistic explanation to the sensitivity of Delta variant to and the increased neutralization potency of this antibody. T478K mutation was located outside the buried surface area without impacting the interaction of Nb22 with RBD of Delta variant, while an additional hydrogen bond, formed by L452R of RBD with T30 of Nb22, possibly contributing to the increased neutralization potency of Nb22 against Delta variant. To the best of our knowledge, Nb22-Fc exhibited one of the highest neutralization potencies among the reported antibodies or nanobodies against Delta variant infection [2, 7, 14, 33, 36]. In view of the global dissemination of the Delta variant, Nb22 will be a potential candidate for the prophylaxis or treatment of the prevalent Delta variant or other circulating variants infection.

Acknowledgements

We thank Prof. Guo. for providing the plasmid of RBD. The X-ray data was collected using Shanghai Synchrotron Radiation Facility on beamline 18U1. This work was supported by National Science Foundation of China (NSFC) (No. 81803414 to X.W.,

31970149 to Z.W.), the Major Research and Development Project (2018ZX10301406 to Z.W.), Ministry of Science and Technology (2020YFA0908500 to S.Y.), the National Natural Science Foundation of China (31971127 to S.Y. and 81801998 to Y.W.), Tianjin Natural Science Foundation (20JCQNJC01570 to Y.W.), Nanjing University-Ningxia University Collaborative Project (Grant# 2017BN04 to Z.W.), Jiangsu Province Natural Science Foundation for Young Scholar (Grant# BK20170653 to X.W.), Key Natural Science Foundation of Jiangsu Province (Grant# ZDA2020014 to X.W.), Jiangsu province "Innovative and Entrepreneurial talent" and Six Talent Peaks Project of Jiangsu Province, the Emergency Prevention and Control Capacity Program for New Severe Infectious diseases of National Institute for Viral Disease Control and Prevention, and the 135 Strategic Program of Chinese Academy of Sciences, the Science and Technology Innovation Committee of Shenzhen Municipality (JCYJ20180228162229889 to L.C.).

Author contributions

XW conducted most experiments, analyzed the data and wrote the draft manuscript. LC conducted all the neutralization experiments. LZ, BH, SX, HS, DZ, LL, WN provided technical assistance. YW and SY conducted structural analysis. ZW designed the study, directed and revised the manuscript. All authors critically reviewed the draft manuscript and approved the final version.

Declaration of interests: The authors declared no competing interests.

Figure Legends

Figure 1 Characterizing nanobodies neutralizing circulating variants of SARS-CoV-2. The neutralization curve of Nb15-Fc (**A**), Nb22-Fc (**B**), Nb31-Fc(**C**) and SNB02 (**D**) inhibiting SARS-CoV-2 pseudovirus of circulating variants. Nb-Fcs and SNB02 were all constructed as the format of VHH fused with human Fc1. SNB02 was taken as an antibody control specific for SFTS virus. (**E)** The summary curve of IC_{50} of Nb-Fcs exhibiting potent neutralization against SARS-CoV-2 variants. (**F**) The summary table of IC_{50} and IC_{80} of Nb-Fcs in A-C, displaying potent neutralization. Data are represented as mean ± SD. All experiments were repeated at least twice.

Figure 2. Characterizing the binding of Nbs. Kinetic binding curve of Nb15-Fc (**A**), Nb22-Fc (**B**) and Nb31-Fc (**C**) at the concentration 33.3 nM,11.1nM, 3.7nM and 1.2 nM with RBD of Delta variant, respectively, detected by BLI. Binding curves are colored black, and fit of the data to a 1:1 binding model is colored red. (**D**) Representative binding curve of various RBD as indicated to Nb22-Fc tested by BLI. Nb22-Fc binding with RBD from representative SARS-CoV-2 variants detected by immunofluorescence assay (**E**) and FACS (**F**), respectively. Mock served as a cell control without plasmid transfection. Images were visualized under the ×10 objective. All experiments were repeated at least twice.

Figure 3. Structural analysis of Nb22 and SARS-CoV-2 RBD complex. (**A**) The overall complex structure of Nb22 and RBD. The CDR1 (red), CDR2 (blue), CDR3 (green) of Nb22 (pink) and RBD (orange) were displayed in cartoon representation. (**B**) The epitope of Nb22 shown in surface representation. The CDR regions were colored in red, blue and green, respectively. The interaction between CDR1 (**C**), CDR2 (**D**), CDR3 (**E**) and RBD. (**F**) The hydrogen bonds of the interface between Nb22 and RBD. The hydrogen bonds were shown in cyan dash line. (**G**) The hydrophobic network between Nb22 and RBD. All the residues were shown in sticks.

Figure 4. Nb22 blocked the binding of ACE2 to RBD. (**A**) Overlap of Nb22 and ACE2 binding sites on RBD. ACE2 binding site on RBD was shown in cyan line, Nb22 binding site was shown in pink line. The overlap region was represented by ellipses with dashed lines. (**B**) The loop (V102-Y117) of Nb22 was clashed with the two helixes on N-terminal of ACE2. The loop was colored in red and helixes were colored in green.

Figure 5. Nb22 potentially resisted the Delta variant (B.1.617.2). (**A**) The two mutation sites of B.1.617.2 in RBD. T478 was located outside the CDR binding regions, L452 was on the CDR2 recognized epitope. L452 and T478 was colored in cyan, epitope of CDRs was colored identical to Fig 1. (B) and (C) Comparison of hydrogen bonds of L452R and T478K mutations. T478K did not affect hydrogen bonds on the interaction interface of Nb22 and RBD. (C) L452R formed an additional hydrogen bond with T30 of Nb22. had relatively little influence on hydrophobic network. The residues

identified were shown in sticks.

Supplemental Materials

Supplemental Table 1. Data collection and refinement statistics

Supplemental Table 2. Hydrogen bonds of the interface between WT or B1.617.2 RBD with Nb22.

Supplemental Table 3. BSA Comparison with reported neutralizing nanobodies.

Figures

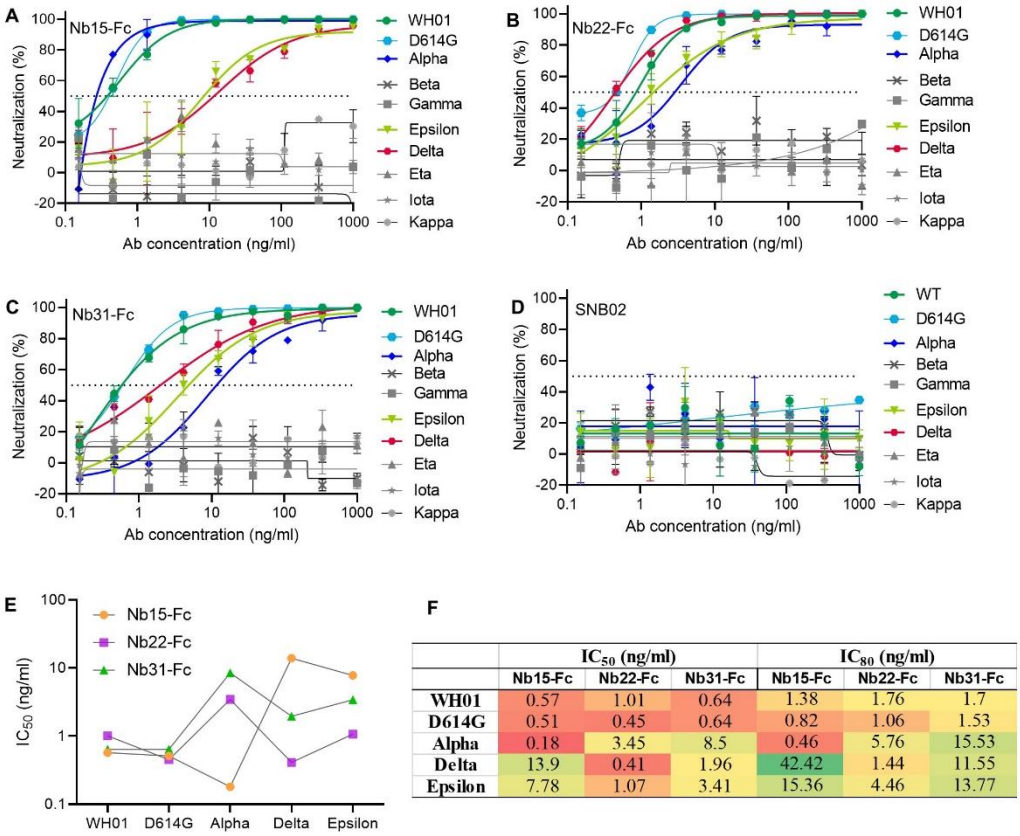

F

	IC_{50} (ng/ml)			IC_{80} (ng/ml)		
	Nb15-Fc	Nb22-Fc	Nb31-Fc	Nb15-Fc	Nb22-Fc	Nb31-Fc
WH01	0.57	1.01	0.64	1.38	1.76	1.7
D614G	0.51	0.45	0.64	0.82	1.06	1.53
Alpha	0.18	3.45	8.5	0.46	5.76	15.53
Delta	13.9	0.41	1.96	42.42	1.44	11.55
Epsilon	7.78	1.07	3.41	15.36	4.46	13.77

Figure 1 Characterizing nanobodies neutralizing circulating variants of SARS-CoV-2. The neutralization curve of Nb15-Fc (**A**), Nb22-Fc (**B**), Nb31-Fc(**C**) and SNB02 (**D**) inhibiting SARS-CoV-2 pseudovirus of circulating variants. Nb-Fcs and SNB02 were all constructed as the format of VHH fused with human Fc1. SNB02 was taken as an antibody control specific for SFTS virus. (**E**) The summary curve of IC_{50} of Nb-Fcs exhibiting potent neutralization against SARS-CoV-2 variants. (**F**) The summary table of IC_{50} and IC_{80} of Nb-Fcs in A-C, displaying potent neutralization. Data are represented as mean ± SD. All experiments were repeated at least twice.

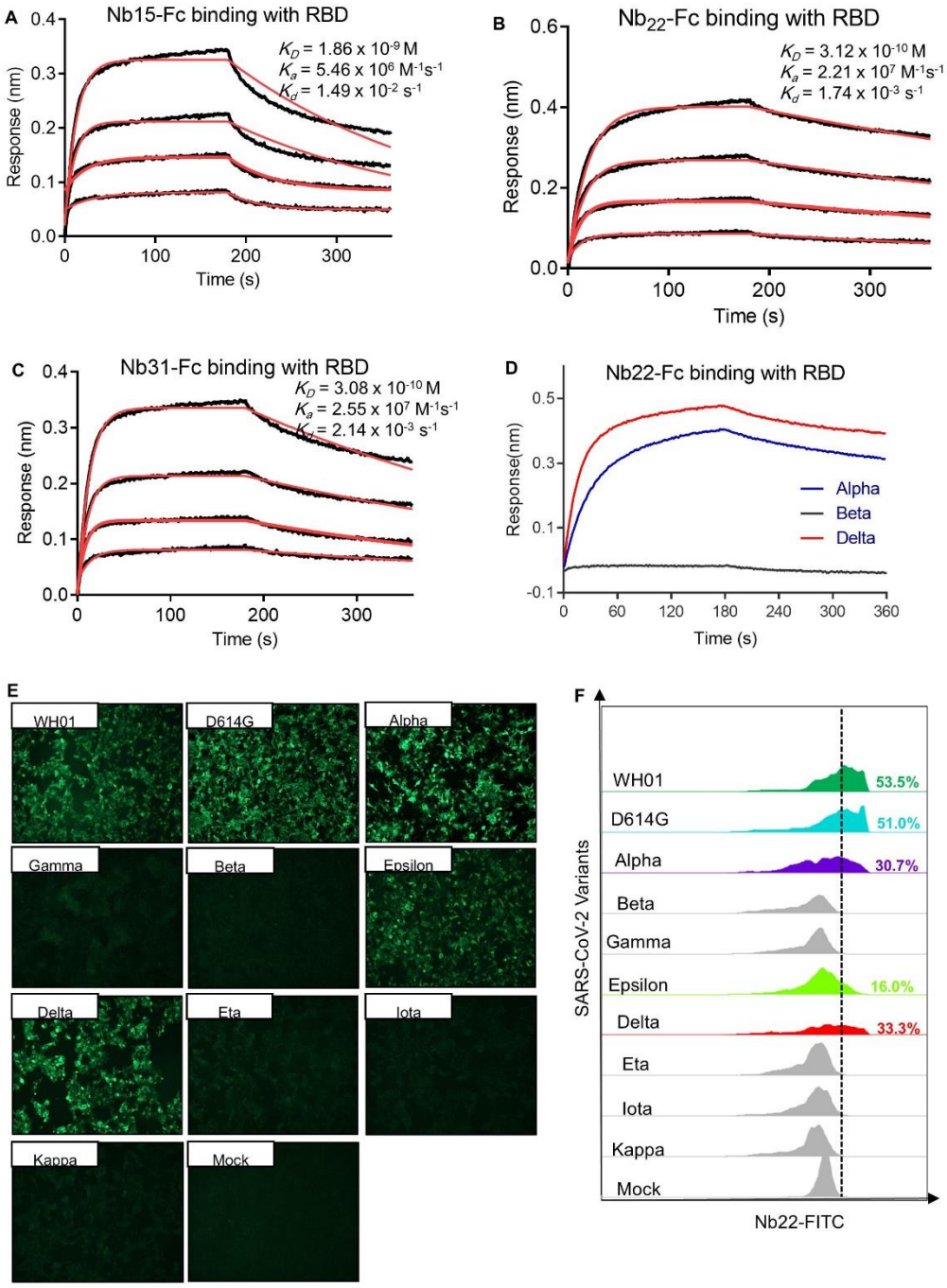

Figure 2. Characterizing the binding of Nbs. Kinetic binding curve of Nb15-Fc (**A**), Nb22-Fc (**B**) and Nb31-Fc (**C**) at the concentration 33.3 nM,11.1nM, 3.7nM and 1.2 nM with RBD of Delta variant, respectively, detected by BLI. Binding curves are colored black, and fit of the data to a 1:1 binding model is colored red. (**D**) Representative binding curve of various RBD as indicated to Nb22-Fc tested by BLI. Nb22-Fc binding with RBD from representative SARS-CoV-2 variants detected by immunofluorescence assay (**E**) and FACS (**F**), respectively. Mock served as a cell

control without plasmid transfection. Images were visualized under the ×10 objective. All experiments were repeated at least twice.

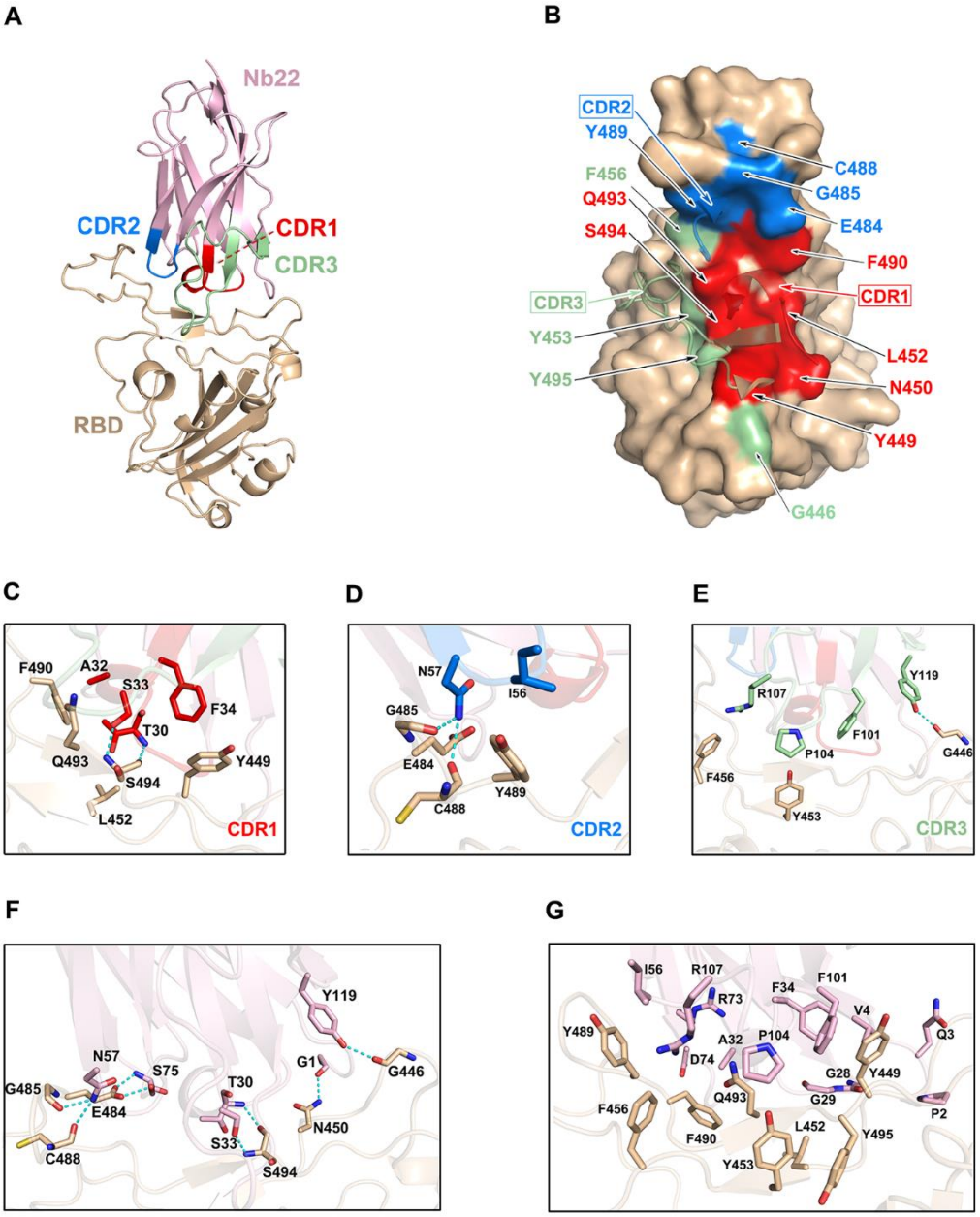

Figure 3. Structural analysis of Nb22 and SARS-CoV-2 RBD complex. (**A**) The overall complex structure of Nb22 and RBD. The CDR1 (red), CDR2 (blue), CDR3 (green) of Nb22 (pink) and RBD (orange) were displayed in cartoon representation. (**B**) The epitope of Nb22 shown in surface representation. The CDR regions were colored

in red, blue and green, respectively. The interaction between CDR1 (**C**), CDR2 (**D**), CDR3 (**E**) and RBD. (**F**) The hydrogen bonds of the interface between Nb22 and RBD. The hydrogen bonds were shown in cyan dash line. (**G**) The hydrophobic network between Nb22 and RBD. All the residues were shown in sticks.

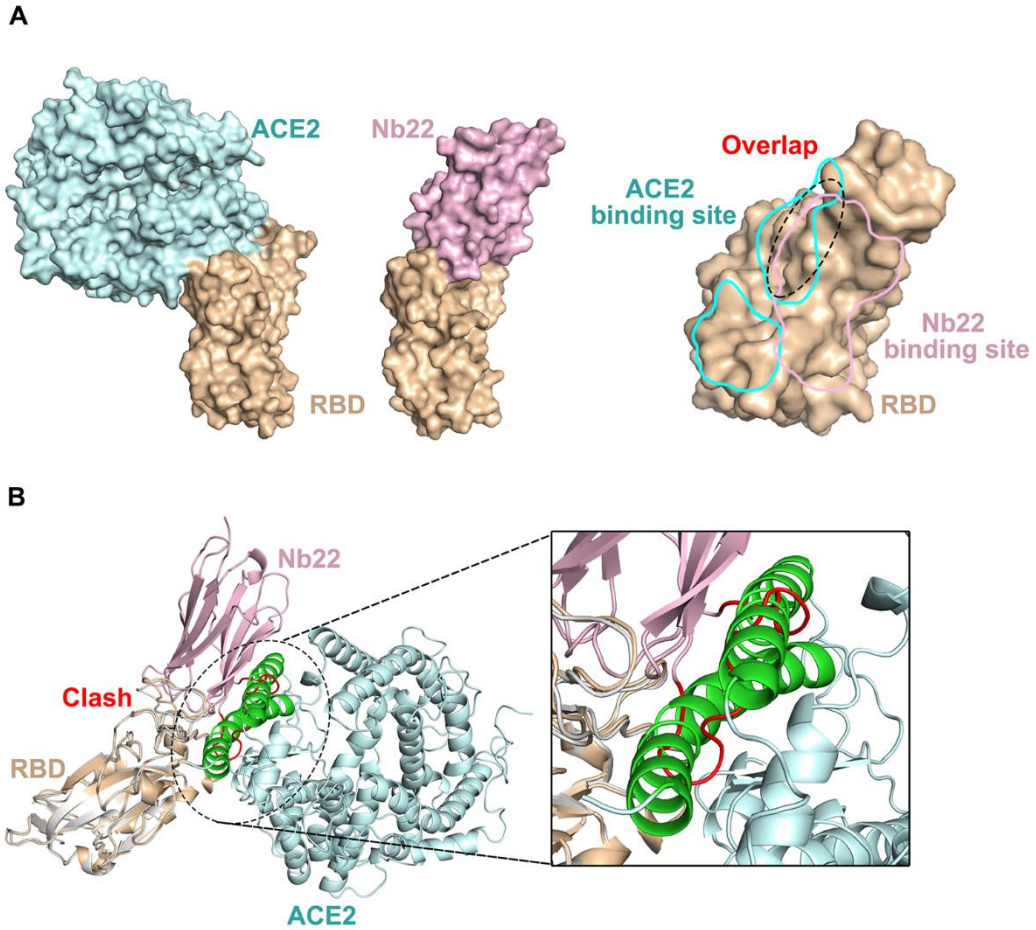

Figure 4. Nb22 blocked the binding of ACE2 to RBD. (**A**) Overlap of Nb22 and ACE2 binding sites on RBD. ACE2 binding site on RBD was shown in cyan line, Nb22 binding site was shown in pink line. The overlap region was represented by ellipses with dashed lines. (**B**) The loop (V102-Y117) of Nb22 was clashed with the two helixes on N-terminal of ACE2. The loop was colored in red and helixes were colored in green.

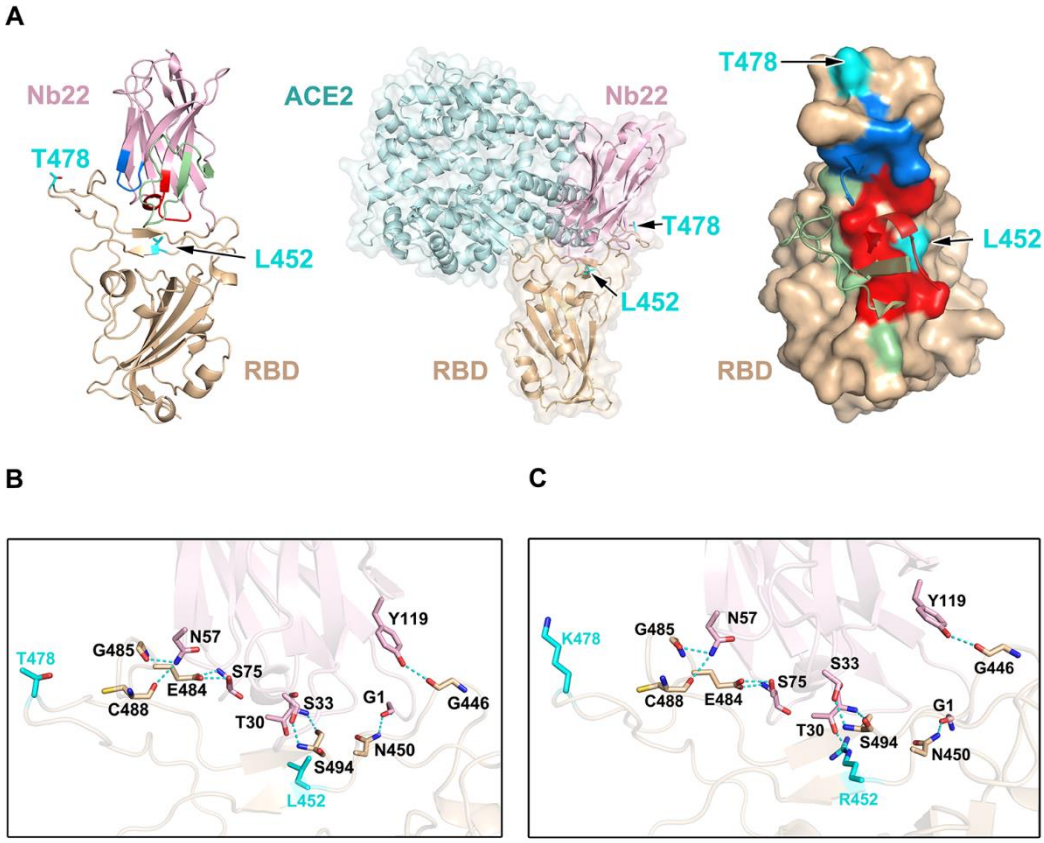

Figure 5. Nb22 potentially resisted the Delta variant (B.1.617.2). (**A**) The two mutation sites of B.1.617.2 in RBD. T478 was located outside the CDR binding regions, L452 was on the CDR2 recognized epitope. L452 and T478 was colored in cyan, epitope of CDRs was colored identical to Fig 1. (B) and (C) Comparison of hydrogen bonds of L452R and T478K mutations. T478K did not affect hydrogen bonds on the interaction interface of Nb22 and RBD. (C) L452R formed an additional hydrogen bond with T30 of Nb22. had relatively little influence on hydrophobic network. The residues identified were shown in sticks.

Reference

1. Zhou, P., et al., *A pneumonia outbreak associated with a new coronavirus of probable bat origin.* Nature, 2020.
2. Liu, C., et al., *Reduced neutralization of SARS-CoV-2 B.1.617 by vaccine and convalescent serum.* Cell, 2021.
3. Garcia-Beltran, W.F., et al., *Multiple SARS-CoV-2 variants escape neutralization by vaccine-induced humoral immunity.* Cell, 2021.

4. Davies, N.G., et al., *Increased mortality in community-tested cases of SARS-CoV-2 lineage B.1.1.7.* Nature, 2021.
5. Plante, J.A., et al., *The variant gambit: COVID-19's next move.* Cell Host & Microbe, 2021. **29**(4): p. 508-515.
6. Bernal, J.L., et al., *Effectiveness of Covid-19 Vaccines against the B.1.617.2 (Delta) Variant.* New England Journal of Medicine, 2021.
7. Planas, D., et al., *Reduced sensitivity of SARS-CoV-2 variant Delta to antibody neutralization.* Nature, 2021.
8. Baum, A., et al., *REGN-COV2 antibodies prevent and treat SARS-CoV-2 infection in rhesus macaques and hamsters.* Science (New York, N.Y.), 2020. **370**(6520): p. 1110-1115.
9. Chen, P., et al., *SARS-CoV-2 Neutralizing Antibody LY-CoV555 in Outpatients with Covid-19.* New England Journal of Medicine, 2020.
10. Farinholt, T., et al., *Transmission event of SARS-CoV-2 Delta variant reveals multiple vaccine breakthrough infections.* medRxiv : the preprint server for health sciences, 2021.
11. Wall, E.C., et al., *Neutralising antibody activity against SARS-CoV-2 VOCs B.1.617.2 and B.1.351 by BNT162b2 vaccination.* Lancet, 2021. **397**(10292): p. 2331-2333.
12. Wall, E.C., et al., *AZD1222-induced neutralising antibody activity against SARS-CoV-2 Delta VOC.* Lancet, 2021. **398**(10296): p. 207-209.
13. Yadav, P.D., et al., *Neutralization of variant under investigation B.1.617 with sera of BBV152 vaccinees.* Clinical infectious diseases : an official publication of the Infectious Diseases Society of America, 2021.
14. Taylor, P.C., et al., *Neutralizing monoclonal antibodies for treatment of COVID-19.* Nature Reviews Immunology, 2021. **21**(6): p. 382-393.
15. Starr, T.N., et al., *Complete map of SARS-CoV-2 RBD mutations that escape the monoclonal antibody LY-CoV555 and its cocktail with LY-CoV016.* Cell Reports Medicine, 2021. **2**(4).
16. Wang, L., et al., *Ultrapotent antibodies against diverse and highly transmissible SARS-CoV-2 variants.* Science (New York, N.Y.), 2021. **373**(6556).
17. Xiang, Y., et al., *Versatile and multivalent nanobodies efficiently neutralize SARS-CoV-2.* Science (New York, N.Y.), 2020. **370**(6523): p. 1479-1484.
18. Schoof, M., et al., *An ultrapotent synthetic nanobody neutralizes SARS-CoV-2 by stabilizing inactive Spike.* Science (New York, N.Y.), 2020. **370**(6523): p. 1473-1479.
19. Huo, J.D., et al., *Neutralizing nanobodies bind SARS-CoV-2 spike RBD and block interaction with ACE2.* Nature Structural & Molecular Biology, 2020. **27**(9): p. 846-+.
20. Hanke, L., et al., *An alpaca nanobody neutralizes SARS-CoV-2 by blocking receptor interaction.* Nature Communications, 2020. **11**(1).
21. Wu, Y., et al., *Identification of Human Single-Domain Antibodies against SARS-CoV-2.* Cell Host & Microbe, 2020. **27**(6): p. 891-+.
22. Dong, J., et al., *Development of multi-specific humanized llama antibodies blocking SARS-CoV-2/ACE2 interaction with high affinity and avidity.* Emerging Microbes & Infections, 2020. **9**(1): p. 1034-1036.
23. Nambulli, S., et al., *Inhalable Nanobody (PiN-21) prevents and treats SARS-CoV-2 infections in Syrian hamsters at ultra-low doses.* Science Advances, 2021. **7**(22).
24. Pymm, P., et al., *Nanobody cocktails potently neutralize SARS-CoV-2 D614G N501Y variant and protect mice.* Proc Natl Acad Sci U S A, 2021. **118**(19).

25. Wu, X., et al., *A potent bispecific nanobody protects hACE2 mice against SARS-CoV-2 infection via intranasal administration.* bioRxiv, 2021: p. 2021.02.08.429275.
26. Wu, X., et al., *A single-domain antibody inhibits SFTSV and mitigates virus-induced pathogenesis in vivo.* JCI Insight, 2020. **5**(13).
27. Huang, B., et al., *Potent Neutralizing Humanized Antibody With Topical Therapeutic Potential Against HPV18-Related Cervical Cancer.* Frontiers in Immunology, 2021. **12**(2339).
28. Minor, W., et al., *HKL-3000: the integration of data reduction and structure solution--from diffraction images to an initial model in minutes.* Acta Crystallogr D Biol Crystallogr, 2006. **62**(Pt 8): p. 859-66.
29. McCoy, A.J., et al., *Phaser crystallographic software.* J Appl Crystallogr, 2007. **40**(Pt 4): p. 658-674.
30. Jin, Z., et al., *Structure of M(pro) from SARS-CoV-2 and discovery of its inhibitors.* Nature, 2020. **582**(7811): p. 289-293.
31. Emsley, P., et al., *Features and development of Coot.* Acta Crystallogr D Biol Crystallogr, 2010. **66**(Pt 4): p. 486-501.
32. Adams, P.D., et al., *PHENIX: a comprehensive Python-based system for macromolecular structure solution.* Acta Crystallogr D Biol Crystallogr, 2010. **66**(Pt 2): p. 213-21.
33. Guttler, T., et al., *Neutralization of SARS-CoV-2 by highly potent, hyperthermostable, and mutation-tolerant nanobodies.* Embo Journal.
34. Wrapp, D., et al., *Structural Basis for Potent Neutralization of Betacoronaviruses by Single-Domain Camelid Antibodies.* Cell, 2020. **181**(6): p. 1436-1441.
35. Starr, T.N., et al., *Complete map of SARS-CoV-2 RBD mutations that escape the monoclonal antibody LY-CoV555 and its cocktail with LY-CoV016.* Cell Rep Med, 2021. **2**(4): p. 100255.
36. Koenig, P.A., et al., *Structure-guided multivalent nanobodies block SARS-CoV-2 infection and suppress mutational escape.* Science, 2021. **371**(6530): p. 691-+.